Mini-Review:

Metal Oxide for Fast Adsorption System in the Methylene Blue Removal

Maria Ulfa[1*], Sukmaningrum Latifah Oktaviani[2], Bakti Mulyani[1], and Novia Amalia Sholeha[3]

[1]*Chemistry Education Study Program, Faculty of Teacher Training and Education, Sebelas Maret University, Jl. Ir. Sutami 36A, Surakarta 57126, Indonesia*

[2]*Magister of Chemistry Education Study Program, Faculty of Teacher Training and Education, Sebelas Maret University, Jl. Ir. Sutami 36A, Surakarta 57126, Indonesia*

[3]*College of Vocational Studies, IPB University, Jl. Kumbang No. 14, Bogor 16151, Indonesia*

* ***Corresponding author:***

email: mariaulfa@staff.uns.ac.id

Received: December 29, 2023
Accepted: November 25, 2024

DOI: 10.22146/ijc.92617

Abstract: *Rapid adsorption systems utilizing metal oxide-based materials represent a promising technology to address adsorption challenges, particularly for the effective removal of methylene blue (MB). These systems enhance the continuous MB elimination process by leveraging metal oxide (MO)-based adsorbents with high accessibility and optimized adsorption conditions. The preparation process involves selecting metal oxides with high surface area and strong adsorbate affinity, ensuring efficient interaction with MB. Process parameters such as adsorbent dosage, contact time, temperature, pH, initial concentration, waste volume, and pressure are modified to develop a rapid and sustainable system for MB removal. This configuration enables efficient application in water treatment, achieving faster and more effective MB degradation. Moreover, the scalability of MO-based adsorbents ensures low-cost production and broad applicability, further supporting sustainable waste management. This review critically evaluates experimental findings from various studies on MO-based materials in rapid adsorption systems, highlighting their potential for large-scale implementation in wastewater treatment to mitigate environmental pollution.*

Keywords: *metal oxide; methylene blue removal; rapid adsorption*

■ INTRODUCTION

Methylene blue (MB) has been considerably utilized in the textile industry as a dyeing agent. Massive usage of MB in industry generates a high dye wastewater due to the rapid enhancement of economic development. Dye wastewater consists of a large number of azo, phenyl, and other organic compounds that are seriously challenging to treat environmental safety. Improper disposal of dye waste can harm the environment and human health [1]. Very high concentrations of MB in water will affect the chromaticity and turbidity of the water. It irritates the skin and nervous system, and long-term absorption of water-contaminated dyes can cause severe damage to the liver and digestive system of the human body [2]. Therefore, a highly efficient removal of MB sewage becomes a significant concern in recent years.

Various strategies have been designed to remove MB in a water environment, including coagulation/flocculation, advanced oxidation process, photodegradation, membrane filtration, adsorption, and biological treatment [3-9]. Among them, adsorption is the most commonly used method for MB removal due to its low operating costs, simple process design, and low contaminant levels [10]. Adsorbents with different properties can be utilized to remove different contaminants [11]. For example, charged inorganic and organic contaminants tend to stick to adsorbents with oppositely charged surfaces due to electrostatic attraction [12]. Heavy metals generally have a high affinity for dyes with abundant surface hydroxyl or other

functional groups. Additionally, adsorption can be reversible so that the adsorbent can be regenerated by appropriate desorption methods [13]. A well-designed sorbent is a core component of the adsorption process. An ideal sorbent for commercial use should possess high adsorption capacity, rapid adsorption kinetics, cost-effectiveness, non-toxicity to the environment, easy separation, robustness, and reusability [14-15].

The use of metal oxides (MOs) in the adsorption of reduced MB is of tremendous interest due to the simplicity and affordability of the approach. As depicted in Fig. 1, the utilization of MO in MB removal has increased for almost years. Especially from 2010 to 2025, the usage of MO in MB adsorption has been significantly enhanced, revealing that MO has an adsorption capability to remove MB. MOs are promising candidates as adsorbents because of their excellent adsorption performance, low cost, easy modification, and regeneration. Using MOs as sorbents to produce high-quality treated wastewater [16], including removing low-concentration contaminants at trace levels, as most naturally polluted waters do not contain some impurities, is essential [17].

According to the description, we reviewed the use of MOs as MB adsorbents. Several types of MO adsorbents are presented to demonstrate their adsorption performance. We summarized the factor-influenced adsorption processes to provide information on how MOs could enhance adsorption performance. Kinetic and reusability analyses were also described to inform the adsorption mechanism using MOs and their potential in long-term adsorption processes. Finally, challenges and prospects are presented in detail.

■ LITERATURE REVIEW

The literature review involved several steps. First, searching for relevant literature, the review process began with an extensive search of scientific databases, such as Scopus, Web of Science, and Google Scholar, to identify studies related to MO adsorbents for MB removal from wastewater. Keywords such as "metal oxide", "adsorption system", "methylene blue removal", and "fast adsorption" were used to gather the most relevant articles. Once the search was complete, articles were selected based on their relevance to the topic. This involved reviewing the abstracts, methods, and results of MOs (e.g., TiO_2, ZnO, Fe_2O_3) for their ability to adsorb MB would be prioritized. The selected articles were then carefully analyzed to extract meaningful data and findings. This included reviewing experimental setups, MO types, adsorption mechanisms, removal efficiencies,

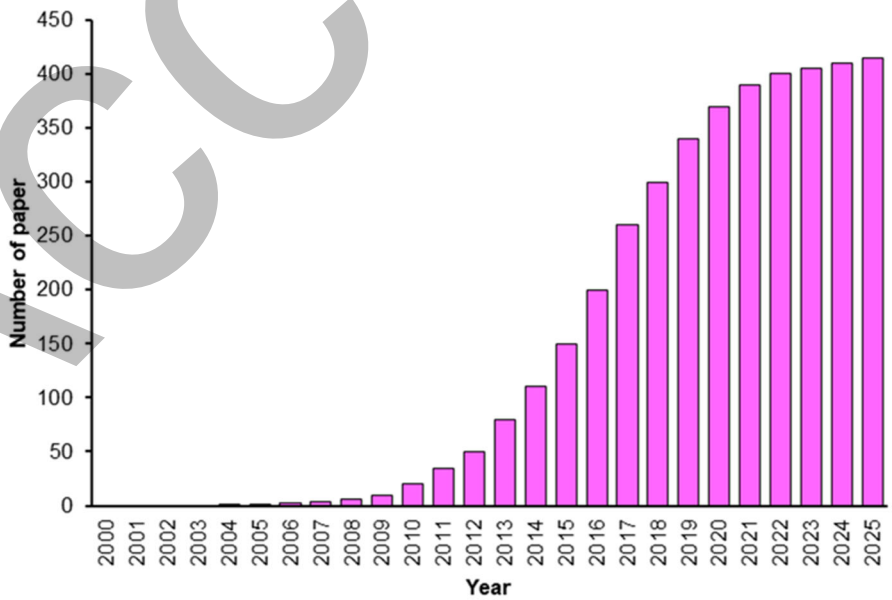

Fig 1. The number of papers regarding the application of MO as MB adsorbent per year from 2000 to 2025, obtained from scopus.com with the keywords "metal oxide for methylene blue"

and factors such as pH, temperature, and adsorbent dosage influencing the adsorption process. The findings from various studies were be compared and synthesized to draw overarching conclusions about the effectiveness of different MOs in MB removal. The goal of this literature survey is to provide a thorough understanding of the field, highlighting the state of the art in MO-based adsorption systems, their advantages, limitations, and potential future directions.

■ TYPE OF METAL OXIDE AS AN ADSORBENT

MO can be used as an adsorbent in three ways, i.e., single metal, bimetal, and multi-metal. Numerous factors lead each study to select one of these kinds. The use of single metals has multiple origins, including verifying the nature of pure metals in removal, particularly in terms of physicochemical stability and decreasing costs, as the use of single metals typically does not necessitate a large number of precursors or complex procedures. However, the decision to utilize a bimetal seems to compensate for the disadvantages of a single metal, as the existence of a bimetal provides an active site that synergistically attracts MB molecules during adsorption. In addition, bimetal is frequently employed to enhance the adsorption process's selectivity, so bimetallic combinations have a high affinity for interacting with MB. Nonetheless, some researchers select multi-metals because there are more opportunities for interactions to occur. Besides, multi-metals can aid each other in increasing the surface area of the contact points and preserving physicochemical stability.

The average MB reduction performance of single metal, bimetal, and multi-metal is determined by the crystalline peak of X-ray diffraction (XRD), the types of precursors, the size of the particles generated, the adsorbent ratio, and the amount of MB pore size, as described in Table 1. Each metal oxide had a crystallinity character detected by XRD at different peaks (Table 1), with an average crystallite size of 10–40 nm (data collecting period 2020-2022) and diverse spherical, ordered, and disordered crystallite morphologies. Depending on the synthesis method, the particle sizes of MO ranged from 10 to 200 nm. Meanwhile, to accomplish optimum adsorption performance, the usual ratio of adsorbent and adsorbate was around 1:4 (w/v). Adsorbents in the form of a single metal, such as ZnO and Fe_2O_3, could reach 99% elimination. Still, several metals had the same ability and highly depended on the pore size, allowing MB access.

Characterization of reference materials was utilized in the selection of MO-based MB adsorbents, including crystalline materials [18]. Although amorphous MO adsorbents are suitable for removing MB, crystalline materials outperform frequently due to a variety of variables. Crystalline materials have well-defined and regular atomic arrangements, which can result in precise adsorption sites for MB molecules. This regular structure may boost the adsorbent's selectivity for MB over other pollutants. Crystalline materials often have a more uniform distribution of adsorption sites, which results in more consistent and predictable adsorption behavior. This homogeneity can increase both adsorption capacity and kinetics. Crystalline materials are often more stable under various circumstances, including temperature, pH, and ionic strength [19]. This stability can lead to a longer service life and more effective reuse of the adsorbent.

Furthermore, a larger surface area means more adsorption sites, which increases adsorption capacity. The suitable pore structure can aid in the passage of MB molecules into the adsorbent, thereby boosting adsorption rates [20]. The adsorbent has consistent particle size distribution. Uniform particle size can improve mass transfer and lower pressure loss in a full-bed reactor [21]. The presence of certain functional groups on the MO surface can either increase or impede MB sorption. For example, hydroxyl groups can promote hydrogen bonding with MB molecules, but carboxyl groups can improve electrostatic interactions [22]. Smaller particle sizes might result in increased surface area and quicker adsorption kinetics. However, homogeneous particle size distribution is essential for constant adsorption efficacy. High adsorption capacity is required for effective MB removal from wastewater. Selectivity is essential for efficient MB removal from complicated wastewater mixtures. The ideal particle size for MO-based MB adsorbents is determined by various criteria,

Table 1. Crystal and morphology features of MO used as MB adsorbent

Sample	XRD peak (°)	Crystallite size (nm)	Precursor	Particle size (nm)	Ratio of samples:MB	Pore size (nm)	Removal (%)	Ref
ZnO	(100), (002), (101), (102), (110), (103), (200)	ND	$Zn(NO_3)_2{\cdot}6H_2O$	100–150	0.1 g:40 mg/L	100	99.00	[1]
FeO NPs	102	37	$FeCl_3$	24-44	3 mg:10 mg/L	ND	90.00	[24]
MnO_2	12.79, 18.05, 28.69, 37.52, 41.95, 49.71, 59.96	34	$KMnO_4$	ND	0.02 g:0.1 g/L	50	93.62	[3]
CuO-Fe_2O_3/CTS-ATP	8.5, 19.5, 27.8, 34.7, 35.4	ND	ATP* wrapped by chitosan as support, $Fe(NO_3)_3{\cdot}9H_2O$ Cu $(NO_3)_2{\cdot}3H_2O$	ND	250 mg/L:1 g/L	14.271	99.29	[4]
CF-15	20–80	ND	$FeCl_3{\cdot}6H_2O$ $CuCl_2{\cdot}2H_2O$	15.6	20 mg:5 mg/L	ND	58.57	[5]
$CaMgO_2$	42	25	$K_3[Fe(CN)_6]$, $CaSO_4$, $MgCl_2$	25	10mg/L:5 mg/L	ND	97.00	[7]
CuO/MCM-41	32.5, 35.5, 38.5, 48.7, 53.5, 58.3, 61.5, 68.1	ND	Cetyltrimethylammonium ammonium bromide, $CuSO_4{\cdot}5H_2O$	21	ND	3–7	97.00	[25]
Cu-Zn-Mn	30.19, 35.48, 53.42, 56.95, 62.51	17.31	$Zn(NO_3)_2{\cdot}6H_2O$ and $Mn(CH_3COO)_2{\cdot}4H_2O$	92.33	ND	ND	87.00	[8]
Fe_2O_3	24.23, 33.25, 35.77, 40.96, 49.58, 54.18, 57.76, 62.55, 64.09, 72.05, 75.57	ND	$Fe(NO_3)_3{\cdot}9H_2O$ L-lysine, L-serine	148.67–201.20 nm	0.15 g:25mg/L	ND	100	[9]
TiO_2	63.01	40.19	TiO_2	ND	0.002 g:3 mg/L	ND	78.00	[10]

*ATP= attapulgite; ND: not determined; NPs: nanoparticles

including desired adsorption capacity, kinetics, and regeneration efficiency [23].

The removal ability of the ZnO and MnO_2 samples in the form of a single metal was greater than that of the Cu-Zn-Mn samples, according to Table 1. Considering the number of active center bonds, the tri-MO (Cu-Zn-Mn) should have a higher adsorption efficiency than the single-type MO. The contact area of the ZnO sample (100–150 nm) was larger than that of the Cu-Zn-Mn sample (92.33 nm). Hence, MB would bind strongly to the large touch area and have several active centers. The difference between the production of single metal oxide and tri-metal oxide lies in the mixing of the three types of MO, as in Cu-Zn-Mn, which is produced by mixing $CuSO_4$, $Zn(NO_3)_2$, and manganese acetate. In contrast, ZnO samples are produced using ultrasonically dispersed $Zn(NO_3)_2$ compounds. The removal ability of modified samples like CuO/MCM-41 (97.00%) and CuO-Fe_2O_3/CTS-ATP (99.29%) was larger than that of pure samples like TiO_2 (78.00%), MnO_2 (93.62%), and ZnO (99.00%). This could be possible because a change can expand the contact area, causing MB to be absorbed and adhere to the larger surface area. MCM-41, which is utilized to alter CuO, has the advantageous effect of enlarging the pore diameter so that MB can be readily captured. Pure MO, such as CuO, have the drawback of agglomeration (clumping) during refining, which reduces the surface area of contact and hence reduces the ability to adsorb MB relative to the modified MO. This is related to the nature of MB, where the higher electronegativity of the MO leads to more MB adhered to the active site; hence, MB will adhere more to Zn than to Mn.

MB adsorption on MO adsorbents is regulated by a number of physical variables, including pore size, crystallinity, particle size, crystallite size, and adsorbent-

to-adsorbate ratio. Mesoporous materials with pore diameters ranging from 2 to 10 nm are often considered ideal for MB adsorption. Larger holes facilitate the diffusion of MB molecules, whereas smaller pores might give more adsorption sites [26]. MOs in crystalline form frequently exhibit superior adsorption capability because of their well-defined structure, which affords particular adsorption sites for MB molecules [27]. MO materials with particle sizes of 100–300 μm are ideal for MB adsorption. Smaller particles enhance the surface area available for adsorption, but they also result in a bigger pressure drop in a full-bed reactor and make separation more challenging [26]. The size of crystallites can have an impact on MO adsorption characteristics. Smaller crystallites may have more surface flaws and active adsorption sites [28]. Higher adsorbent-to-adsorbate ratios can enhance MB removal performance while increasing treatment costs. Higher ratios give more adsorption sites for MB molecules; thus, increasing total adsorption capacity. Higher ratios can boost adsorption rates by shortening the diffusion route for MB molecules. Higher ratios may result in higher removal percentages from wastewater [29].

■ MB ADSORPTION FACTORS VIA METAL OXIDE ADSORBENT

Physical factors such as crystallinity, particle size, crystallite size, and the adsorbent-to-adsorbate ratio greatly impact the MO's ability to absorb MB. However, secondary elements are just as significant in determining the best circumstances for MB elimination. Table 2 examines the surface area factor, pore diameter, starting concentration, adsorbent weight, adsorbate volume, and the type of functional group present in MOs. It seems to deepen the internal parameters (such as surface area and functional groups) directly related to the adsorption process and external adsorption factors (such as the variable C_0, adsorbent mass, adsorbate volume, and time).

According to Table 2, single metals have a smaller surface area (80 m^2/g) than metals scattered on other materials, such as carbon, due to the tendency of MOs to form agglomerates between 5 and 20 nm in size. This is why some researchers chose to distribute the MO on the supporting material so that the MO's performance could be enhanced by the cost-effectiveness and equal distribution of small particle sizes. In addition, the adsorption period for both pure and modified MOs from Table 2 ranged from 50 to 240 min, where not all long adsorption times resulted in a significant amount of MB elimination. There are numerous reasons for these phenomena. One of which is that some forms of adsorbate are not strong enough to attract the other adsorbate, causing the bound adsorbate to be released and recombine with the bulk adsorbate solution upon long-term adsorption. Due to the support of supporting materials, ZnO was able to achieve over 93% elimination in a short time (between 30 and 50 min) [12,14]. The rapid

Table 2. MB adsorption performance on MO

Sample	S (m^2/g)	D (nm)	Time (min)	C_0 (mg/L)	m (g)	V (mL)	Removal (%)	Ref
AC-CuO	5.9082	14.6344	50	5	0.200	ND	95.28	[11]
AC-ZnO	4.9138	17.1305			0.050		94.95	
AC-TiO_2	7.8951	15.6531			0.300		96.96	
ZnO	20.460	2–10	50	ND	0.600	150	98.17	[12]
CuO	25.760	ND	120	ND	ND	100	88.00	[13]
ZnO	63.264	10–20	30	10	1.000	100	94.12	[14]
Fe_2TiO_5/BC	656.00	ND	120	ND	0.025	50	36.00	[15]
TiO_2	50.400	8.8000	60	ND	0.020	100	97.90	[16]
TiO_2–MCTs	264.58	18.0500	60	10	0.020	200	91.00	[17]
TiO_2 film	ND	ND	240	3	ND	80	78.00	[10]
SnO_2	5.6475	4.6934	60	ND	0.050	50	78.00	[30]
CuO/g-C_3N_4	ND	ND	100	50	0.100	100	94.00	[31]

S: surface area; D: diameter; C_0: initial concentration; m: mass; V: volume

adsorption system with a time range of 10 to 60 min is favored by many researchers and industries because of its cost-, labor-, and energy-saving benefits. Although ZnO, as a single metal without a supporting material, has a high adsorption capacity due to its relatively high surface area compared to other MOs, the necessary adsorbent mass of 1 g is rather significant. Even though ZnO is effective in terms of time, the enormous amount of adsorbent required necessitates important prices, particularly during manufacture. This leads us to select a different type of MO, such as TiO_2, which takes relatively little adsorbent to remove MB with a relatively high removal rate (about 97%), which is likely owing to the correct volume ratio of adsorbent-to-adsorbate. In ZnO investigations (Table 2), when the adsorbate volume was increased from 100 to 150 mL, the removal percentage rose by 5%. This can be a consideration for optimizing the adsorption process so that the physical features of the adsorbent fit the external adsorption conditions, with the keywords time efficiency, adsorbent weight, initial adsorbate concentration, and adsorbate volume being crucial.

Modification of MO will boost MB removal because it will increase the contact area. MB will be confined in the active center on the touch area as in the TiO_2 film samples. Table 2 shows that TiO_2 thin film and TiO_2-MCTs had MB removal capacities of 78% and 91%, respectively. For this reason, TiO_2 modified with MCTs can have a greater pore diameter because MCTs are particularly porous materials; hence, they will absorb more MB than thin-film TiO_2 samples. This also occurred with AC-CuO (95.28%) and CuO (88.00%) samples. Based on Table 2, most samples were exposed to MB for 50 to 60 min. Nevertheless, an excessively extended soaking time will also hinder the removal capability. Microporous blockage inhibits the elimination of MB from the sample. The stronger a metal's electronegativity causes the metal to adhere to MB more readily. This is consistent with the comparison of ZnO and CuO samples, in which the removal percentage of ZnO (98.17%) was greater than that of CuO (88.00%), as Zn is more electronegative than Cu. However, the adsorption capacity of MB is significantly influenced by the physicochemical properties of the adsorbent.

Additionally, the surface charge nature of the adsorbent is critical to investigate to improve the MB attachment. An adsorbent with a negative surface charge is advantageous for MB adsorption due to the positive nature of MB molecules in an aqueous medium. For instance, combining TiO_2 with ZSM-5 exhibits a negative surface nature, which is suitable for creating electrostatic attractions with MB molecules [12]. To improve performance, pH adjustment is greatly considered to obtain the optimum performance of MB adsorption. As reported by Lu et al. [30], MB adsorption using Fe-Mn binary oxide exhibited a low adsorption efficiency at acidic conditions, revealing that the surface charge of Fe-Mn binary oxide was positive at acidic conditions. The positive surface charge of Fe-Mn binary oxide leads to proton adsorption since the molecule size of the proton is smaller than that of MB molecules, creating an electrostatic repulsion with MB molecule and reducing the adsorption result. However, the MB adsorption at alkaline conditions is plateaued since the pH zero point charge of Fe-Mn binary oxide is 6.2. Mrunal et al. reported the enhancement of MB adsorption results in alkaline conditions using Cu_2O [19]. Similarly, Liu et al. also exposed a significant improvement in adsorption performance from a pH of 3 to 9, followed by a slight increase after a pH of 9 using MnO_2-modified lignin biochar [32]. Typically, MO has a negatively charged surface in alkaline conditions, promoting the MB molecule attachment on its surface and improving the results.

The rapid adsorption system is inextricable from the selected synthesis technique for producing MO or MO-based adsorbents with exceptional physicochemical properties. The low quality of the MO before and after modification by traditional or advanced methods, which are ineffective and inefficient in terms of process complexity, cost, power, and energy, is the impetus for the method selection. Compared to polymerization, sol-gel, and precipitation, hydrothermal technique has typically been favored the most. Each process utilized multiple precursors, including metal nitrates (e.g., $Zn(NO_3)_2{\cdot}6H_2O$, $Ce(NO_3)_3{\cdot}6H_2O$, and $Ni(NO_3)_2$), metal salts (e.g., $Ti(OC_4H_9)_4$), and metal carbonates (e.g.,

$CdCO_3$). Each precursor has unique features, and the average selection criterion is the ease with which the precursor may be transformed into impurity-free MO. Some of the usual hydrothermal template routes use both soft and hard templates, such as wood templates and sporopollenin exine capsules. For time spent in the reactor's aging chamber, the chosen hydrothermal range was between 2 and 20 h, with decomposition/calcination temperatures averaging between 60–700 °C. It is believed that the selection of various aging times is strongly related to the necessity for MOs to develop at varying degrees of crystallinity. A low decomposition temperature and aging time may be necessary to reduce energy and labor consumption during synthesis.

Based on Table 3, the soft template approach employing poly(*N*-isopropyl acrylamide) (PNIPAM) provided the most effective MO with moderate aging times and calcination temperatures. Having an N group to attract MB is related to the need for mild circumstances in the structural arrangement. This N group is quite sensitive. By joining organic groups in MOs, most employed templates contain crosslinked organic groups, such as lycopodium, PNIPAM, and methylate. Based on the calcination temperature range, the most utilized MO was between 300 and 700 °C, with the majority being calcined at temperatures over 600 °C for an average of 3 h. Water was the predominant solvent utilized in MOs. The hydrothermal process was the method of choice for producing MOs to improve physicochemical qualities and MB removal performance. Even so, the adsorption kinetics test remains an essential metric for determining the response rate of MB elimination; therefore, a method based on a kinetic model should not be overlooked.

■ KINETIC MODEL OF MB ADSORPTION ON METAL OXIDE

Kinetic modeling not only permit the calculation of the sorption rate, but it also yields a rate expression that matches the parameters of a potential reaction mechanism. Several kinetic models, such as pseudo-first-order kinetic models, pseudo-second-order kinetic models, and intraparticle diffusion models, were examined in this context. The pseudo-first-order Lagergren model is predicated on the assumption that the rate of change of solute uptake with time is directly proportional to the difference between saturation concentration and amount of solid uptake with time, which is generally true during the initial stages of the

Table 3. Synthesis method of MO for MB adsorption

Samples	Methods	Precursor templates	Aging time (h)	Temperature (°C)	Solvent	Removal (%)	Ref.
Ni-doped iron oxide	Hydrothermal	PNIPAM, $Ni(NO_3)_2$, $FeSO_4$	12	200	Milli Q water	99.00	[32]
CdO	Precipitation	MICP (microbially induced cadmium precipitation), $CdCO_3$	20	450	ND	78.00	[33]
ZnO/SAPO-34 (AC-U)	Hydrothermal	$Zn(NO_3)_2{\cdot}6H_2O$ and NaOH	3	300	Deionized water	95.70	[34]
CeO_2	Hydrothermal	Lycopodium-pollen-templated CeO_2	3	700	Deionized water	ND	[35]
CTAB-Mo-TiO_2/FAC	Sol-gel	Commercial fly ash cenospheres (FAC), $Ti(OC_4H_9)_4$	2	500	Ethanol	99.70	[10]
Fe_2O_3	Hydrothermal	Lycopodium-pollen-templated Fe_2O_3	3	700	Deionized water	ND	[35]
CeO_2	hydrothermal	$Ce(NO_3)_3{\cdot}6\ H_2O$	4	450	Deionized water	90.00	[36]
m-PDA-PMMA/SnO_2	*In-situ* polymerization process	PMMA, SnO_2	5	70	THF solvent	95.30	[37-38]
TiO_2	Hydrothermal	$Ti(OC_4H_9)_4$	3	260–600	Ethanol, deionized water, and glacial acetic acid	97.90	[16]
ZnO	Hydrothermal	$Zn(NO_3)_2{\cdot}6\ H_2O$	20	160	Deionized water	94.15	[31]

adsorption process [11,39-40]. In the graph of ln [absorption] along the y-axis vs time along the x-axis, the outcome is a straight line with the slope m = - k' and the intersection b = ln (absorbance). Therefore, the slope measured from the graph yields the desired number, the apparent rate constant (k'). The pseudo-second-order model is a rate-limiting step where surface adsorption involves physicochemical interactions between adsorbents in addition to chemisorption [11,40-41]. Various prior studies regard these two models as the most illustrative of the adsorption kinetics model.

The pseudo-second-order model is commonly used to characterize adsorption kinetics, notably for MB on different adsorbents. This model implies that the rate-determining phase is chemisorption, which is the creation of chemical bonds between the adsorbate (MB) and the adsorbent [41]. MB is a cationic dye that interacts electrostatically with negatively charged functional groups on the adsorbent surface, including carboxylates, sulfates, and phosphates. This electrostatic attraction causes the development of strong chemical bonds, which is compatible with the chemisorption process proposed by the pseudo-second-order model [42]. While the pseudo-second-order model is commonly used to describe monolayer adsorption, it may also account for multilayer development under certain situations. If MB molecules stack or aggregate on the adsorbent surface, the total adsorption rate increases, resulting in a better fit to the pseudo-second-order model [43]. The pseudo-second-order model does not explicitly account for intraparticle diffusion. Still, it can offer a fair match to experimental data if this process is faster than the chemisorption step. In other words, if the MB molecules can diffuse into the adsorbent pores without encountering considerable resistance, the chemical interaction at the surface will have the greatest influence on the total adsorption rate [44]. The adsorption kinetics can be influenced by experimental parameters, such as adsorbent dose, starting MB concentration, and temperature. For example, increasing the adsorbent dose can increase the accessible surface area for MB adsorption, resulting in quicker rates and a better fit to the pseudo-second-order model [45]. The physical and chemical features of the adsorbent, such as surface area, pore size distribution, and functional group density, can all influence adsorption kinetics. Adsorbents having a large surface area and numerous functional groups are more likely to display pseudo-second-order kinetics due to their improved capacity to interact with MB molecules [46].

The adsorption of MB by MO-based materials predominantly follows the pseudo-second-order kinetic model rather than the pseudo-first-order model, with an average linearity of 0.982–0.999, as shown in Table 4. The k' value fluctuates between 10^{-4} and 10^{-2} $(mol/L)^{1-n}$ s^{-1}, representing the specific rate of the reaction, linking the reaction rate to the concentration of the reactants. A smaller value of k' indicates a faster reaction. MO materials combined with biochar, such as Fe_2TiO_5/BC and MnO_2-BC, exhibit the highest k', which can be attributed to the high surface area and the strong affinity of MOs for the biochar support. Both samples not only accelerated the decay rate but also achieved the highest adsorption capacity among other MOs. The adsorption process was reportedly independent of the available porosity of the support and provided more surface interaction due to a moderate initial concentration-to-MB volume ratio, ranging from 4:1 to 1:1 (w:v), with an adsorbent weight of 25–50 mg and an approximate adsorption time of 180 min. Although the reaction time is relatively long, the required adsorbent amount is small, and the reaction rate reaches maximum adsorption capacity, thereby improving the overall efficiency of MB removal on a large scale.

Table 4 shows that capacity decreased as the w/v increased. The ratio between 3 and 8 then reduced precipitously. Therefore, the capacity will fall if the ratio increases. Then, based on time, if the time decreases, the capacity also declines. The new capacity will increase if the experiment is conducted for more than 100 min, indicating that the time balance is greater than 100 min. From Table 4, MO without combination or modification tended to have a lower capacity than the combination of other materials. The shorter equilibrium duration, as in the M-Burkeana-Fe_3O_4 material (30 min equilibrium), means that the fast adsorption system is more effective, with the proviso that this equilibrium is stable and there

is no issue of the adsorbate detaching from the adsorbent and recombining with the mother liquid.

■ REGENERATION OF METAL OXIDE-BASED ADSORBENT ON MB ADSORPTION

The adsorbent regeneration method involves delivering spent adsorbent material and connecting it with a solvent composition to assist in the removal of adsorbate, contaminants, and impurities from the primary material. Because the reuse of adsorbents substantially reduces prices, labor, and energy without the complication of re-synthesizing adsorbents, regeneration is the cornerstone of the world's hope for the eradication of MB waste worldwide. Numerous investigations on adsorbent renewal (thermal, chemical, microbiological, and vacuum regeneration) have been conducted to improve adsorption efficiency. On the surface of the adsorbent, organic contaminants can be transformed into harmless molecules. MO-based adsorbents can be regenerated to recover their MB-removal capacity. Although previous studies have examined the removal of MB with various adsorbents, no specific research has compared regeneration parameters (such as type of regeneration method, type of solvent, regeneration conditions, time, and temperature) with the total ability to remove MB in several cycles, as shown in Table 5.

Table 4. Kinetic model of MB adsorption on MO

Sample	Model	K'	q_e	R^2	C_0 (mg/L)	W (g)	V (mL)	t (min)	Ref.
Biochar ZnO	PSO	0.001	146.2	0.982	160	0.100	100	225	[47]
Fe_2TiO_5/BC	PSO	9.217×10^{-4}	229.9	0.980	100	0.025	25	180	[15]
RGO-TiO_2-CdO-ZnO-Ag	PFO	0.062	ND	0.950	ND	0.500	10	15	[48]
MnO_2-BC	PSO	7.324×10^{-4}	167.1	0.999	50	ND	50	180	[49]
CeO_2-g-C_3N_3	PSO	0.232	ND	0.982	ND	0.050	100	180	[50]
Fe_2O_3 NPs	PSO	0.063	50	0.999	20	0.400	50	45	[51]
Fe_3O_4	PSO	0.033	29.82	0.999	100	1	300	100	[52]
CuO@AC	PSO	0.037	29.31	0.987	10	0.100	50	60	[53]
CoO_x-ACs	PFO	0.029	ND	0.990	100	0.100	500	60	[54]
M-Burkeana-Fe_3O_4	PFO	0.096	ND	0.990	5	0.025	100	30	[55]

PFO: pseudo-first-order; PSO: pseudo-second-order; q_e: equilibrium adsorption capacity; k': rate constant; t: adsorption time; q_t: adsorption capacity at a certain time

Table 5. Regeneration of adsorbent-based MO on MB adsorption

Sample	Method	Solvent	Ratio of solvent:material	t (h)	T (°C)	Removal percentage in cycles (%)							Ref
						1st	2nd	3rd	4th	5th	6th	7th	
Fe_3O_4-OPBC-NCs	Batch	HCl and NaOH	ND	4	30	61.0	ND	ND	ND	48.8	-	-	[55]
α-MnO_2/Fe-Mn BO	Batch	NaOH	100 mL: 0.0013 g	12	30	97.2	92.3	88.3	80.3	74.2	64.7	52.3	[55]
Ce-Mn-Co	Batch	H_2O_2	20 mL: 20 mg	12	100	99.0	97.0	95.0	85.0	77.4	-	-	[56]
magnetic Fe_3O_4/TiO_2/graphene sponge (MFTGS)	Batch	Ethanol	ND	ND	ND	91.0	89.0	81.0	81.0	-	-	-	[57]
GO-MnO_2	ND	Deionized water	ND	ND	ND	99.0	98.7	98.5	96.0	95.0	93.0	-	[58]
CuO-[p(NiPmA-mAc)]	ND	Deionized water	ND	ND	ND	100	99.0	95.0	90.0	-	-	-	[59]
$MgFe_2O_4$/rGO	Batch	NaOH	ND	0.167	100	78.0	75.0	70.0	-	-	-	-	[60]
AC-CuO	Batch	HCl and NaOH	ND	ND	ND	100	88.8	79.5	62.3	-	-	-	[11]
AC-ZnO	Batch	HCl and NaOH	ND	ND	ND	97.9	91.9	66.6	45.7	-	-	-	[11]
AC-TiO_2	Batch	HCl and NaOH	ND	ND	ND	99.3	96.7	66.9	24.0	-	-	-	[11]

Each MO-based adsorbent has a distinct ability to regenerate. MnO_2-based bimetallic material could regenerate up to 7 cycles with a total removal of MB of about 550 mg/g or a steady average removal of 79 mg/g per cycle with a procedure that reduces the removal ability by approximately 5%/cycle. This will not be found in materials exhibiting a decline in removal ability in the first four cycles, such as activated carbon (AC)-MO composite samples (AC-CuO, AC-ZnO, AC-TiO_2) that can remove 330 mg/g with a decrease in removal capacity of approximately 20%/cycle. Under mild settings, the temperature of the support for preparing the post-regeneration adsorbent was between room temperature and 120 °C for 1 to 24 h. The removal of ZnO as a single metal was twice greater than that of an AC composite (such as AC-CuO, AC-ZnO, and AC-TiO_2). This is anticipated from the selected MO, composite, and regeneration processes. MnO_2/Fe-Mn BO is an example of a bimetallic adsorbent that appears more stable after repeated use when compared to AC-CuO composites. Bimetallic materials typically retain their stability following regeneration.

Furthermore, the regeneration mechanism determines the material's ability to remain stable after multiple cycles. The batch method has been the most common technique since it is less complicated than thermal breakdown methods and other adsorbate release techniques. Nonetheless, double solvents such as HCl-NaOH in the batch approach appeared to reduce the removal capability by up to 20% compared to the batch method using a single solvent. In the first two cycles, alkaline substances such as NaOH decreased removal capacity by approximately 4%, whereas solvent peroxide reduced removal ability by 2%. This demonstrates that dilute peroxide tends to stabilize the material when removing MB without causing considerable harm. However, the batch peroxide approach is typically avoided to protect the environment from excessive peroxide discharge due to its toxicity. However, the ratio of the recycled adsorbent to the amount of solvent must be re-evaluated. A minimal amount of solvent is optimal because it decreases the amount of solvents used in regeneration. These considerations should be taken into account when selecting a regeneration procedure to extend the material's useful life.

As seen in Table 5, many solvents are NaOH because it helps eliminate MB. NaOH possesses a potent extractive ability to remove organic groups from MOs. NaOH is not detrimental to bimetallic metals but is more destructive to multi-metallic metals. Still, this compound can also slowly dissolve MOs, causing the substance to deteriorate. Several studies have also employed H_2O_2 as a solvent for MOs. H_2O_2 offers both advantages and problems. The benefit of H_2O_2 is that it has two hydrogen bonds, allowing it to bind MB strongly. It also does not damage the material because it decomposes into H_2O and O_2. However, if H_2O_2 is discarded, it will become hazardous waste.

Fig. 2 corresponds to specific interactions or components within the adsorption mechanism. MB will dissociate in an aqueous solution (solvent) at the onset of adsorption and then continue to interact with the cation portion of the adsorbent to a certain extent. According to numerous researchers, the adsorption mechanism of MB in the adsorbent depends on all the forces acting between the adsorbent-adsorbate particles, where, under balanced conditions, not all adsorbent surfaces are surrounded by adsorbate atoms or ions. This phenomenon is referred to as partial covering. Although both batches and continuous adsorption techniques are employed for a variety of applications, including MB removal, batch approaches are more extensively researched and addressed in the literature. This is because batch experiments employ a well-mixed, static system and are often easier to set up and control. Factors such as adsorbent dose, starting MB concentration, and temperature may be more easily adjusted in a batch system. Batch experiments are useful for investigating adsorption kinetics, equilibrium isotherms, and understanding processes [61]. Data from batch experiments may be used to create and evaluate mathematical models of the adsorption process. Flow rate, mixing, and adsorbent renewal can all hinder the transition from batches to continuous operations. Continuous systems frequently need more complicated equipment and control systems, which can raise operating

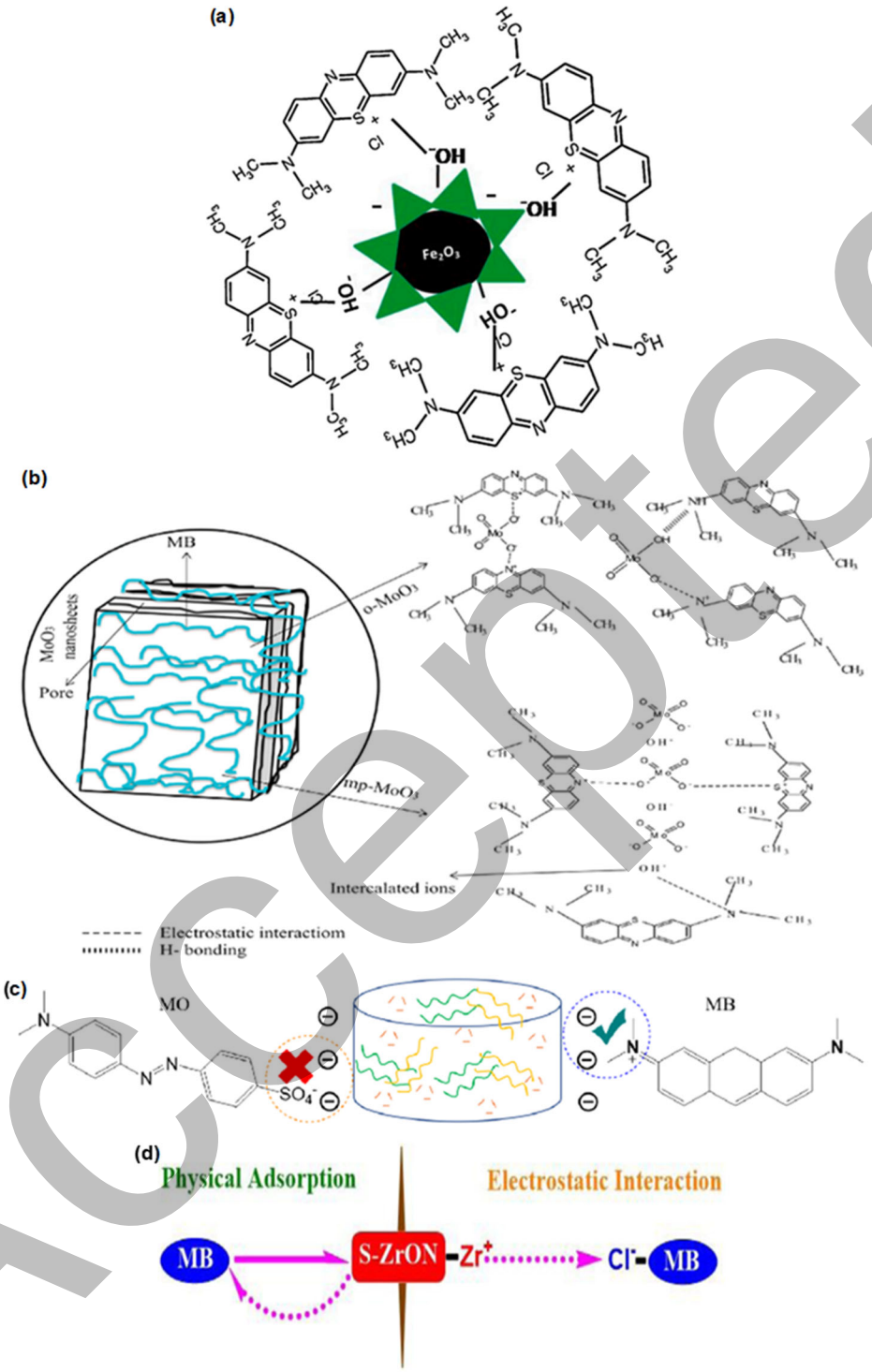

Fig 2. Mechanism of MB adsorption using (a) Fe_2O_3 NPs [51], (b) Mp-MoO_3 o-MoO_3 [81], (c) C/SA/Fe [82], and (d) S-ZrON [83]

costs and complexity. Many research investigations focus on understanding adsorption's underlying mechanics and dynamics, which are sometimes easier to explore via batch experiments. Batch tests can be performed to determine the viability of utilizing a certain adsorbent for MB removal before scaling up to continuous operation [62].

One of the factors of partial covering is the size of the adsorbate. The size prevents the adsorbate from accessing the narrow surface area. The affinity of the adsorbent surface can also be another factor that does not provide a functional group that attracts the adsorbate. Another one is the presence of steric hindrance due to overlapping adsorbates, such that one adsorbate prevents the interaction of other adsorbates with the surface contact area of the adsorbent. Several earlier research have identified a variety of adsorption processes for MB.

The definition of adsorption technique is a mass transfer procedure in which one or more substances (adsorbate) in a gas or liquid stream are selectively transported to a porous solid surface (adsorbent). Several aspects influence the rate of absorption. The extent of adsorption on a solid surface is determined by the following factors, i.e., adsorbent qualities, surface area, gas properties, exothermic properties, and pressure. One of the factors that increase absorption is surface area. The greater surface area of the solid adsorbent permits more adsorption. Additionally, the lower particle size results in a larger surface area. Adsorption rises as the pressure of the adsorbate increases, and this increase is the most significant at low temperatures.

The adsorption of MB on composite adsorbents, such as MO-carbon hybrid materials, involves complex chemical interactions that are crucial for understanding the efficiency of the process. As seen in Table 6, the most commonly proposed mechanisms for MB adsorption are electrostatic interactions and hydrogen bonding. MOs, such as TiO_2, ZnO, and CuO, typically carry negative charges on their surfaces, enabling electrostatic attraction formation with the positively charged MB molecules. These interactions are significant in the initial stages of adsorption, as the positive charge on MB facilitates its binding to the anionic sites of the MO surfaces. The extent of this interaction can be influenced by the specific surface properties and the charge distribution on the adsorbent, which vary with different types of MO-based composites [63].

Hydrogen bonding, another critical interaction in adsorption, often arises between the hydroxyl groups on the adsorbent surfaces and the MB molecules. This is especially pronounced in composite adsorbents that incorporate carbon nanotubes, graphene oxide, or other hydrophilic components. The formation of hydrogen bonds with the –OH groups on the adsorbent's surface leads to the establishment of strong adsorption sites, making the process faster and more efficient [64-65]. These interactions are confirmed through shifts in the FTIR spectra, where the broadening of the –OH stretching band and peak intensity variations indicate hydrogen bonds' involvement in MB adsorption. The synergy between electrostatic forces and hydrogen bonding interactions significantly enhances the adsorption capacity of these composites [66-67].

Additionally, conjugated π-π interactions between aromatic groups in the adsorbent, such as graphene oxide or carbon nanotubes, and the aromatic rings in MB contribute to the adsorption process [68-69]. These interactions further enhance the adsorption efficiency, particularly when composite materials that combine MOs

Table 6. Interaction between MB on MO-based composite during adsorption

Sample	[MB](mg/L)	Interactions	Ref
TiO_2@SiO_2 nanoparticles	10	Electrostatic, hydrogen bonding	[63]
Hematite α-Fe_2O_3 nanoparticles	10	Electrostatic, π···π stacking, hydrogen bonding	[64]
ZnO Nanoparticles	20	Electrostatic	[65]
Biochar@Al_2O_3 nanocomposite	20	Electrostatic, hydrogen bonding	[66]
Co_3O_4/WO_3/GO	5	Electrostatic, hydrogen bonding	[67]
$Mg(NO_3)_2$-modified lignite-based adsorbent	300	Electrostatic, π···π stacking	[68]
CuO Nanoparticles	10	Electrostatic, hydrogen bonding	[69]
Fe_3O_4@SiO_2 magnetic nanoparticles	10	Electrostatic	[70]
CeO_2/TiO_2 nanotubes	15	Hydrogen bonding, electrostatic	[71]
Fe_3O_4/SnO_2 nanocomposites	20	Electrostatic, π···π stacking	[72]

with carbon-based materials are used. The interplay between these interactions—electrostatic attraction, hydrogen bonding, and π-π interactions—offers a multi-faceted approach to the removal of MB from aqueous solutions. The ability to engineer adsorbents that efficiently exploit these interactions is vital for improving the speed and capacity of adsorption, which is essential for practical applications in water treatment and environmental cleanup. As researchers continue to fine-tune the design of composite adsorbents, achieving a balance between these interaction mechanisms will be key to optimizing MB removal under varying environmental conditions [70-71].

Generally, the evaluation of how the adsorption of MB happens on the surface of the adsorbent is conducted by comparing the adsorbent's features before and after adsorption. After adsorption, components such as N, S, and Na often correlate with the presence of MB in the composite structure. Several sorts of interactions have been proposed in Fig. 2 to explain the adsorption of MB on MO-based adsorbents, but two pathways appear to be the most likely. Electrostatic interactions between the metal oxide anion group (O^{2-}) and the filler and the positive charge of MB or the positive charge of MO with the cation component of MB provide the initial chance for MB adsorption. The second possibility is the result of hydrogen bonding between the adsorbent hydroxide and MB. This is confirmed by the broadening of the signal at 3419 cm^{-1} due to the –OH group in FTIR spectra, which indicates a novel hydrogen bond interaction between MB and MO-based adsorbents. Peak shift from 1616 to 1601 cm^{-1} and 1419 to 1412 cm^{-1} (due to the stretching of MOs caused by MB addition) and the increase in peak intensity in the aforementioned regions can be attributed to the electrostatic involvement of these functional groups in the MB adsorption [72]. Due to the MB adsorption by the MO-support material, such as carbon in the C/Sa/Fe composite, a conjugated structure and - interaction can be observed between the adsorbent and MB. Hydrogen interaction is anticipated to play the most significant function in the fast adsorption method because it offers the most hope for the rapid non-release of MB from the mother liquor. Support electrostatic interactions and conjugated structure interaction from the supporting material continue to play a significant role so long as there is no competition or overlapping molecules between the adsorbate molecules, allowing all contact surfaces of the adsorbent to function efficiently. This leaves significant work to be done to engineer an adsorbent with sufficient accessibility to accommodate 1–2 nm MB without the risk of competition and overlapping but capable of absorbing waste in a relatively short time if the ratio of the weight to the volume of the adsorbent and the adsorbate concentration is immense. If this is accomplished, it is hoped that the fast adsorption system will become the method of choice for large-scale organic waste processing that is cheap, effective, and efficient.

To summarize, mesoporous silica [73] and MO composites have shown great promise in various applications, particularly in the MB adsorption [74-75]. Recent studies have emphasized the crucial role of structural properties and synthesis methods in improving material performance for environmental applications, such as wastewater treatment. For example, advancements in the design of mesoporous silica with low iron concentrations and composites supported on gelatin have demonstrated enhanced adsorption capacities [76-78]. These findings underscore the importance of systematic literature reviews and continued exploration to understand material behavior better, ultimately guiding the development of more efficient materials for real applications [79-80].

■ CONCLUSION

A synthetic method approach to improve the physicochemical properties of the adsorbent was evaluated based on the results of XRD, FTIR, adsorption-desorption nitrogen, and MB adsorption performance to describe the sustainable condition of this MO-based adsorption. For the adsorbent preparation procedures, the template approach is a quick and eco-friendly route that delivers considerable physicochemical performance and increases the chemical resistance of the adsorbent in favor of stability

after regeneration. Single metal structures and multi-MO-based composites have distinct adsorption capacities. Here, two vital and current topics in the adsorption process, phenomenological studies and the shape of the linear kinetic model for MB adsorption, are explored in depth, leading to the conclusion that MB adsorption largely follows a pseudo-second-order model. The evaluation of the comparison between the linear adsorption isotherm forms of the kinetic model for the adsorption of MB reveals that the adsorbent with the highest adsorption rate is a bimetallic adsorbent with a removal rate greater than 93%. Other parameters, such as low adsorbent weight, short adsorption duration, high adsorbate volume, and high starting concentration of MB, can be used as a reference to reduce adsorption costs and labor. The fast adsorption system that takes these two factors into account will be an environmentally friendly, effective, efficient, and safe method, meaning that the release of MB into the environment will not harm waters with high regeneration properties and that it can be reused for multiple times.

■ ACKNOWLEDGMENTS

The authors would like to thank Universitas Sebelas Maret for funding this research through the international collaboration grant under contract number 194.2/UN27.22/PT.01.03/2024.

■ CONFLICT OF INTEREST

The authors confirm that there is no conflict of interest to declare.

■ AUTHOR CONTRIBUTIONS

Conceptualization: Maria Ulfa and Sukmaningrum Latifah Oktaviani; methodology: Maria Ulfa; software: Maria Ulfa, Bakti Mulyani and Novia Amalia Sholeha; formal analysis: Maria Ulfa and Sukmaningrum Latifah Oktaviani; investigation: Maria Ulfa and Bakti Mulyani; data curation: Maria Ulfa and Sukmaningrum Latifah Oktaviani writing—original draft preparation: Maria Ulfa and Sukmaningrum Latifah Oktaviani; writing—review and editing: Maria Ulfa and Novia Amalia Sholeha; visualization, supervision, project administration, and funding acquisition: Maria Ulfa. All authors have read and agreed to the published version of the manuscript.

■ REFERENCES

[1] Liu, X., Wang, G., Zhi, H., Dong, J., Hao, J., Zhang, X., Wang, J., Li, D., and Liu, B., 2022, Synthesis of the porous ZnO nanosheets and TiO_2/ZnO/FTO composite films by a low-temperature hydrothermal method and their applications in photocatalysis and electrochromism, *Coatings*, 12 (5), 695.

[2] Jamshaid, M., Khan, A.A., Ahmed, K., and Saleem, M., 2018, Heavy metal in drinking water its effect on human health and its treatment techniques – A review, *Int. J. Biosci.*, 12 (4), 223–240.

[3] Ahmed, S., Ahmad, Z., Kumar, A., Rafiq, M., Vashistha, V.K., Ashiq, M.N., and Kumar, A., 2021, Effective removal of methylene blue using nanoscale manganese oxide rods and spheres derived from different precursors of manganese, *J. Phys. Chem. Solids*, 155, 110121.

[4] Zhang, T., Li, W., Guo, Q., Wang, Y., and Li, C., 2022, Preparation of a heterogeneous catalyst CuO-Fe_2O_3/CTS-ATP and degradation of methylene blue and ciprofloxacin, *Coatings*, 12 (5), 559.

[5] Haider, S., Shar, S.S., Shakir, I., and Agboola, P.O., 2022, Visible light active Cu-doped iron oxide for photocatalytic treatment of methylene blue, *Ceram. Int.*, 48 (6), 7605–7612.

[6] Karuppusamy, I., Samuel, M.S., Selvarajan, E., Shanmugam, S., Sahaya Murphin Kumar, P., Brindhadevi, K., and Pugazhendhi, A., 2021, Ultrasound-assisted synthesis of mixed calcium magnesium oxide ($CaMgO_2$) nanoflakes for photocatalytic degradation of methylene blue, *J. Colloid Interface Sci.*, 584, 770–778.

[7] ur Rehman, K., Zaman, U., Khan, D., and Khan, W.U., 2022, Surfactant assisted CuO/MCM-41 nanocomposite: Ultra efficient photocatalyst for degradation of methylene blue dye and inactivation of highly drug resistant bacteria, *Mater. Chem. Phys.*, 277, 125454.

[8] Alam, M.W., Al Qahtani, H.S., Souayeh, B., Ahmed, W., Albalawi, H., Farhan, M., Abuzir, A., and

Naeem, S., 2022, Novel copper-zinc-manganese ternary metal oxide nanocomposite as heterogeneous catalyst for glucose sensor and antibacterial activity, *Antioxidants*, 11 (6), 1064.

[9] Subaihi, A., and Naglah, A.M., 2022, Facile synthesis and characterization of Fe_2O_3 nanoparticles using L-lysine and L-serine for efficient photocatalytic degradation of methylene blue dye, *Arabian J. Chem.*, 15 (2), 103613.

[10] Shilpa, G., Mohan Kumar, P., Kishore Kumar, D., Deepthi, P.R., Sukhdev, A., and Bhaskar, P., 2022, A rutile phase-TiO_2 film via a facile hydrothermal method for photocatalytic methylene blue dye decolourization, *Mater. Today: Proc.*, 62, 5477–5482.

[11] Li, J., Han, L., Zhang, T., Qu, C., Yu, T., and Yang, B., 2022, Removal of methylene blue by metal oxides supported by oily sludge pyrolysis residues, *Appl. Sci.*, 12 (9), 4725.

[12] Venkatesan, S., Suresh, S., Ramu, P., Kandasamy, M., Arumugam, J., Thambidurai, S., Prabu, K.M., and Pugazhenthiran, N., 2022, Biosynthesis of zinc oxide nanoparticles using *Euphorbia milii* leaf constituents: Characterization and improved photocatalytic degradation of methylene blue dye under natural sunlight, *J. Indian Chem. Soc.*, 99 (5), 100436.

[13] Ahmad, A., Khan, M., Khan, S., Luque, R., Abualnaja, K.M., Alduaij, O.K., and Yousef, T.A., 2022, Bio-construction of CuO nanoparticles using Texas sage plant extract for catalytical degradation of methylene blue via photocatalysis, *J. Mol. Struct.*, 1256, 132522.

[14] He, X., Yang, Y., Li, Y., Chen, J., Yang, S., Liu, R., and Xu, Z., 2022, Effects of structure and surface properties on the performance of ZnO towards photocatalytic degradation of methylene blue, *Appl. Surf. Sci.*, 599, 153898.

[15] Herath, A., Navarathna, C., Warren, S., Perez, F., Pittman, C.U., and Mlsna, T.E., 2022, Iron/titanium oxide-biochar (Fe_2TiO_5/BC): A versatile adsorbent/photocatalyst for aqueous Cr(VI), Pb^{2+}, F^- and methylene blue, *J. Colloid Interface Sci.*, 614, 603–616.

[16] Yang, T., Liu, Y., Xia, G., Zhu, X., and Zhao, Y., 2021, Degradation of formaldehyde and methylene blue using wood-templated biomimetic TiO_2, *J. Cleaner Prod.*, 329, 129726.

[17] Guo, J., Fan, Y., Dong, X., Ma, X., Yao, S., and Xing, H., 2021, Modified coal tailings with TiO_2 nanotubes and their application for methylene blue removal, *Colloids Surf., A*, 627, 127211.

[18] Calimli, M.H., Nas, M.S., Burhan, H., Mustafov, S.D., Demirbas, Ö., and Sen, F., 2020, Preparation, characterization and adsorption kinetics of methylene blue dye in reduced-graphene oxide supported nanoadsorbents, *J. Mol. Liq.*, 309, 113171.

[19] Mrunal, V.K., Vishnu, A.K., Momin, N., and Manjanna, J., 2019, Cu_2O nanoparticles for adsorption and photocatalytic degradation of methylene blue dye from aqueous medium, *Environ. Nanotechnol. Monit. Manage.*, 12, 100265.

[20] Akhtar, F., Andersson, L., Ogunwumi, S., Hedin, N., and Bergström, L., 2014, Structuring adsorbents and catalysts by processing of porous powders, *J. Eur. Ceram. Soc.*, 34 (7), 1643–1666.

[21] Suresh Kumar, P., Korving, L., Keesman, K.J., van Loosdrecht, M.C.M., and Witkamp, G.J., 2019, Effect of pore size distribution and particle size of porous metal oxides on phosphate adsorption capacity and kinetics, *Chem. Eng. J.*, 358, 160–169.

[22] Lu, H., Qi, Y., Zhao, Y., and Jin, N., 2018, Effects of hydroxyl group on the interaction of carboxylated flavonoid derivatives with *S. cerevisiae* α-glucosidase, *Curr. Comput.-Aided Drug Des.*, 16 (1), 31–44.

[23] Partlan, E., Ren, Y., Apul, O.G., Ladner, D.A., and Karanfil, T., 2020, Adsorption kinetics of synthetic organic contaminants onto superfine powdered activated carbon, *Chemosphere*, 253, 126628.

[24] Abid, M.A., Abid, D.A., Aziz, W.J., and Rashid, T.M., 2021, Iron oxide nanoparticles synthesized using garlic and onion peel extracts rapidly degrade methylene blue dye, *Phys. B*, 622, 413277.

[25] Hachemaoui, M., Boukoussa, B., Mokhtar, A., Mekki, A., Beldjilali, M., Benaissa, M., Zaoui, F., Hakiki, A., Chaibi, W., Sassi, M., and Hamacha, R., 2020, Dyes adsorption, antifungal and antibacterial properties of metal loaded mesoporous silica: Effect

of metal and calcination treatment, *Mater. Chem. Phys.*, 256, 123704.

[26] Liu, M., Dong, J., Wang, W., Yang, M., Gu, Y., and Han, R., 2019, Study of methylene blue adsorption from solution by magnetic graphene oxide composites, *Desalin. Water Treat.*, 147, 398–408.

[27] Ai, L., Zhang, C., and Chen, Z., 2011, Removal of methylene blue from aqueous solution by a solvothermal-synthesized graphene/magnetite composite, *J. Hazard. Mater.*, 192 (3), 1515–1524.

[28] Yang, Z., 2008, Kinetics and mechanism of the adsorption of methylene blue onto ACFs, *J. China Univ. Min. Technol.*, 18 (3), 437–440.

[29] Largitte, L., and Pasquier, R., 2016, A review of the kinetics adsorption models and their application to the adsorption of lead by an activated carbon, *Chem. Eng. Res. Des.*, 109, 495–504.

[30] Lu, K., Wang, T., Zhai, L., Wu, W., Dong, S., Gao, S., and Mao, L., 2019, Adsorption behavior and mechanism of Fe-Mn binary oxide nanoparticles: Adsorption of methylene blue, *J. Colloid Interface Sci.*, 539, 553–562.

[31] Phuruangrat, A., Kuntalue, B., Thongtem, S., and Thongtem, T., 2021, Hydrothermal synthesis of hexagonal ZnO nanoplates used for photodegradation of methylene blue, *Optik*, 226 (Part 1), 165949.

[32] Liu, J., Zhou, L., Dong, F., and Hudson-Edwards, K.A., 2017, Enhancing As(V) adsorption and passivation using biologically formed nano-sized FeS coatings on limestone: Implications for acid mine drainage treatment and neutralization, *Chemosphere*, 168, 529–538.

[33] Martínez, C.M., Acosta-Rodríguez, I., Gutiérrez-Sánchez, M., Ruíz, F., and Compeán-García, V.D., 2022, Novel green route synthesis of CdO nanostructures by using $CdCO_3$ obtained by MICP and its application in photodegradation of methylene blue and Congo red, *Sustainable Chem. Pharm.*, 27, 100611.

[34] Ebrahimi, A., Haghighi, M., and Aghamohammadi, S., 2022, Sono-precipitation fabrication of ZnO over modified SAPO-34 zeotype for effective degradation of methylene blue pollutant under simulated solar light illumination, *Process Saf. Environ. Prot.*, 165, 307–322.

[35] Shin, J., Andreas Hutomo, C., Kim, J., Jang, J., and Park, C.B., 2022, Natural pollen exine-templated synthesis of photocatalytic metal oxides with high surface area and oxygen vacancies, *Appl. Surf. Sci.*, 599, 154064.

[36] Cheng, Z., Luo, S., Liu, Z., Zhang, Y., Liao, Y., Guo, M., and Nguyen, T.T., 2022, Visible-light-driven hierarchical porous CeO_2 derived from wood for effective photocatalytic degradation of methylene blue, *Opt. Mater.*, 129, 112429.

[37] Vijayakumar, T.P., Benoy, M.D., Duraimurugan, J., Suresh Kumar, G., Shkir, M., Maadeswaran, P., Senthil Kumar, A., and Ramesh Kumar, K.A., 2022, Hydrothermal synthesis of CuO/g-C_3N_4 nanosheets for visible-light driven photodegradation of methylene blue, *Diamond Relat. Mater.*, 121, 108735.

[38] Alkayal, N.S., Altowairki, H., Alosaimi, A.M., and Hussein, M.A., 2022, Network template-based cross-linked poly(methyl methacrylate)/tin(IV) oxide nanocomposites for the photocatalytic degradation of MB under UV irradiation, *J. Mater. Res. Technol.*, 18, 2721–2734.

[39] Yuh-Shan, H., 2004, Citation review of Lagergren kinetic rate equation on adsorption reactions, *Scientometrics*, 59 (1), 171–177.

[40] Gomes, A.L.M., Andrade, P.H.M., Palhares, H.G., Dumont, M.R., Soares, D.C.F., Volkringer, C., Houmard, M., and Nunes, E.H.M., 2021, Facile sol–gel synthesis of silica sorbents for the removal of organic pollutants from aqueous media, *J. Mater. Res. Technol.*, 15, 4580–4594.

[41] Wu, F.C., Tseng, R.L., Huang, S.C., and Juang, R.S., 2009, Characteristics of pseudo-second-order kinetic model for liquid-phase adsorption: A mini-review, *Chem. Eng. J.*, 151 (1-3), 1–9.

[42] Van Hung, N., Nguyet, B.T.M., Nghi, N.H., Thanh, N.M., Quyen, N.D.V., Nguyen, V.T., Nhiem, D.N., and Khieu, D.Q., 2023, Highly effective adsorption of organic dyes from aqueous solutions on longan seed-derived activated carbon, *Environ. Eng. Res.*, 28 (3), 220116.

[43] Al-Odayni, A.B., Alsubaie, F.S., Abdu, N.A.Y., Al-Kahtani, H.M., and Saeed, W.S., 2023, Adsorption kinetics of methyl orange from model polluted water onto N-doped activated carbons prepared from N-containing polymers, *Polymers*, 15 (9), 1983.

[44] Lach, J., and Okoniewska, E., 2024, Equilibrium, kinetic, and diffusion mechanism of lead(II) and cadmium(II) adsorption onto commercial activated carbons, *Molecules*, 29 (11), 2418.

[45] Jaseela, P.K., Garvasis, J., and Joseph, A., 2019, Selective adsorption of methylene blue (MB) dye from aqueous mixture of MB and methyl orange (MO) using mesoporous titania (TiO_2) – poly vinyl alcohol (PVA) nanocomposite, *J. Mol. Liq.*, 286, 110908.

[46] Neves, C.V., Módenes, A.N., Scheufele, F.B., Rocha, R.P., Pereira, M.F.R., Figueiredo, J.L., and Borba, C.E., 2021, Dibenzothiophene adsorption onto carbon-based adsorbent produced from the coconut shell: Effect of the functional groups density and textural properties on kinetics and equilibrium, *Fuel*, 292, 120354.

[47] Yu, F., Tian, F., Zou, H., Ye, Z., Peng, C., Huang, J., Zheng, Y., Zhang, Y., Yang, Y., Wei, X., and Gao, B., 2021, ZnO/biochar nanocomposites via solvent free ball milling for enhanced adsorption and photocatalytic degradation of methylene blue, *J. Hazard. Mater.*, 415, 125511.

[48] Akyüz, D., 2021, rGO-TiO_2-CdO-ZnO-Ag photocatalyst for enhancing photocatalytic degradation of methylene blue, *Opt. Mater.*, 116, 111090.

[49] Liu, X.J., Li, M.F., and Singh, S.K., 2021, Manganese-modified lignin biochar as adsorbent for removal of methylene blue, *J. Mater. Res. Technol.*, 12, 1434–1445.

[50] Wei, X., Wang, X., Pu, Y., Liu, A., Chen, C., Zou, W., Zheng, Y., Huang, J., Zhang, Y., Yang, Y., Naushad, M., Gao, B., and Dong, L., 2021, Facile ball-milling synthesis of CeO_2/g-C_3N_4 Z-scheme heterojunction for synergistic adsorption and photodegradation of methylene blue: Characteristics, kinetics, models, and mechanisms, *Chem. Eng. J.*, 420, 127719.

[51] Jain, A., Wadhawan, S., and Mehta, S.K., 2021, Biogenic synthesis of non-toxic iron oxide NPs via *Syzygium aromaticum* for the removal of methylene blue, *Environ. Nanotechnol., Monit. Manage.*, 16, 100464.

[52] Wu, K.H., Huang, W.C., Hung, W.C., and Tsai, C.W., 2021, Modified expanded graphite/Fe_3O_4 composite as an adsorbent of methylene blue: Adsorption kinetics and isotherms, *Mater. Sci. Eng., B*, 266, 115068.

[53] Farooq, S., Al Maani, A.H., Naureen, Z., Hussain, J., Siddiqa, A., and Al Harrasi, A., 2022, Synthesis and characterization of copper oxide-loaded activated carbon nanocomposite: Adsorption of methylene blue, kinetic, isotherm, and thermodynamic study, *J. Water Process Eng.*, 47, 102692.

[54] Murugesan, A., Loganathan, M., Senthil Kumar, P., and Vo, D.V.N., 2021, Cobalt and nickel oxides supported activated carbon as an effective photocatalysts for the degradation methylene blue dye from aquatic environment, *Sustainable Chem. Pharm.*, 21, 100406.

[55] Mahlaule-Glory, L.M., Mapetla, S., Makofane, A., Mathipa, M.M., and Hintsho-Mbita, N.C., 2022, Biosynthesis of iron oxide nanoparticles for the degradation of methylene blue dye, sulfisoxazole antibiotic and removal of bacteria from real water, *Heliyon*, 8 (9), e10536.

[56] Wang, Q., Deng, W., Lin, X., Huang, X., Wei, L., Gong, L., Liu, C., Liu, G., and Liu, Q., 2021, Solid-state preparation of mesoporous Ce–Mn–Co ternary mixed oxide nanoparticles for catalytic degradation of methylene blue, *J. Rare Earths*, 39 (7), 826–834.

[57] Maimaiti, T., Hu, R., Yuan, H., Liang, C., Liu, F., Li, Q., Lan, S., Yu, B., and Yang, S.T., 2022, Magnetic Fe_3O_4/TiO_2/graphene sponge for the adsorption of methylene blue in aqueous solution, *Diamond Relat. Mater.*, 123, 108811.

[58] Verma, M., Tyagi, I., Kumar, V., Goel, S., Vaya, D., and Kim, H., 2021, Fabrication of GO–MnO_2 nanocomposite using hydrothermal process for cationic and anionic dyes adsorption: Kinetics,

isotherm, and reusability, *J. Environ. Chem. Eng.*, 9 (5), 106045.

[59] Din, M.I., Khalid, R., and Hussain, Z., 2022, Novel in-situ synthesis of copper oxide nanoparticle in smart polymer microgel for catalytic reduction of methylene blue, *J. Mol. Liq.*, 358, 119181.

[60] Adel, M., Ahmed, M.A., and Mohamed, A.A., 2021, Synthesis and characterization of magnetically separable and recyclable crumbled $MgFe_2O_4$/reduced graphene oxide nanoparticles for removal of methylene blue dye from aqueous solutions, *J. Phys. Chem. Solids*, 149, 109760.

[61] Bahrami, M., Amiri, M.J., Rajabi, S., and Mahmoudi, M., 2024, The removal of methylene blue from aqueous solutions by polyethylene microplastics: Modeling batch adsorption using random forest regression, *Alexandria Eng. J.*, 95, 101–113.

[62] Malbenia John, M., Benettayeb, A., Belkacem, M., Ruvimbo Mitchel, C., Hadj Brahim, M., Benettayeb, I., Haddou, B., Al-Farraj, S., Alkahtane, A.A., Ghosh, S., Chia, C.H., Sillanpaa, M., Baigenzhenov, O., and Hosseini-Bandegharaei, A., 2024, An overview on the key advantages and limitations of batch and dynamic modes of biosorption of metal ions, *Chemosphere*, 357, 142051.

[63] Mahanta, U., Khandelwal, M., and Deshpande, A.S., 2022, TiO_2@SiO_2 nanoparticles for methylene blue removal and photocatalytic degradation under natural sunlight and low-power UV light, *Appl. Surf. Sci.*, 576, 151745.

[64] Goudjil, M.B., Dali, H., Zighmi, S., Mahcene, Z., and Bencheikh, S.E., 2024, Photocatalytic degradation of methylene blue dye with biosynthesized hematite α-Fe_2O_3 nanoparticles under UV-irradiation, *Desalin. Water Treat.*, 317, 100079.

[65] Ahmadi, S., and Igwegbe, C.A., 2020, Removal of methylene blue on zinc oxide nanoparticles: Nonlinear and linear adsorption isotherms and kinetics study, *Sigma J. Eng. Nat. Sci.*, 38 (1), 289–303.

[66] Ameen, S., Hussain, Z., Din, M.I., Khan, R.U., and Khalid, R., 2024, Green synthesis of biochar@Al_2O_3 nanocomposite from waste *Melia azedarach* fruit biomass pyrolysis: A sustainable solution for photocatalytic methylene blue dye degradation, *Desalin. Water Treat.*, 320, 100609.

[67] Alharbi, K.H., 2024, Efficient removal of methylene blue from aqueous solutions using mixed oxides of cobalt oxide and tungsten trioxide modified graphene oxide, *J. Saudi Chem. Soc.*, 28 (1), 101802.

[68] Bai, R., Feng, Y., Wu, L., Li, N., Liu, Q., Teng, Y., He, R., Zhi, K., Zhou, H., and Qi, X., 2023, Adsorption mechanism of methylene blue by magnesium salt-modified lignite-based adsorbents, *J. Environ. Manage.*, 344, 118514.

[69] Essa, W.K., 2024, Methylene blue removal by copper oxide nanoparticles obtained from green synthesis of *Melia azedarach*: Kinetic and isotherm studies, *Chemistry*, 6 (1), 249–63.

[70] Lei, Y., Zhang, X., Meng, X., and Wang, Z., 2022, The preparation of core–shell Fe_3O_4@SiO_2 magnetic nanoparticles with different surface carboxyl densities and their application in the removal of methylene blue, *Inorg. Chem. Commun.*, 139, 109381.

[71] Tuyen, L.T.T., Quang, D.A., Tam Toan, T.T., Tung, T.Q., Hoa, T.T., Mau, T.X., Hoa, T.T., Mau, T.X., and Khieu, D.Q., 2018, Synthesis of CeO_2/TiO_2 nanotubes and heterogeneous photocatalytic degradation of methylene blue, *J. Environ. Chem. Eng.*, 6 (5), 5999–6011.

[72] Paramarta, V., Taufik, A., and Saleh, R., 2017, The role of annealing temperature in photocatalytic performance of Fe_3O_4/SnO_2 nanocomposites, *IOP Conf. Ser.: Mater. Sci. Eng.*, 196 (1), 012032.

[73] Ulfa, M., and Setiarini, I., 2022, The effect of zinc oxide supported on gelatin mesoporous silica (GSBA-15) on structural character and their methylene blue photodegradation performance, *Bull. Chem. React. Eng. Catal.*, 17 (2), 363–374.

[74] Utubira, Y., Wijaya, K., Triyono, T., and Sugiharto, E., 2006, Preparation and characterization of TiO_2-zeolite and its application to degrade textille wastewater by photocatalytic method, *Indones. J. Chem.*, 6 (3), 231–237.

[75] Lhimr, S., Bouhlassa, S., and Ammary, B., 2019, Effect of molar ratio on structural and size of ZnO/C nanocomposite synthesized using a

colloidal method at low temperature, *Indones. J. Chem.*, 19 (2), 422–429.

[76] Ulfa, M., Pangestuti, I., and Anggreani, C.N., 2024, Physicochemical characteristics of titania particles synthesized with gelatin as a template before and after regeneration and their performance in photocatalytic methylene blue, *Bull. Chem. React. Eng. Catal.*, 19 (2), 242–251.

[77] Ulfa, M., Prasetyoko, D., Mahadi, A.H., and Bahruji, H., 2020, Size tunable mesoporous carbon microspheres using Pluronic F127 and gelatin as co-template for removal of ibuprofen, *Sci. Total Environ.*, 711, 135066.

[78] Ulfa, M., and Purnama Ali, M.A., 2022, Influence of calcination temperatures on gunningite-based gelatin template and its application as ibuprofen adsorption, *Indones. J. Chem.*, 22 (6), 1684–1692.

[79] Ulfa, M., Trisunaryanti, W., Falah, I.I., and Kartini, I., 2016, Wormhole-like mesoporous carbons from gelatine as multistep infiltration effect, *Indones. J. Chem.*, 16 (3), 239–242.

[80] Ulfa, M., Nina, N., Pangestuti, I., Holilah, H., Bahruji, H., Rilda, Y., Alias, S.H., and Nur, H., 2024, Enhancing photocatalytic activity of Fe_2O_3/TiO_2 with gelatin: A fuzzy logic analysis of mesoporosity and iron loading, *S. Afr. J. Chem. Eng.*, 50, 245–260.

[81] Kumar, N., and Kumar, R., 2022, Efficient adsorption of methylene blue on hybrid structural phase of MoO_3 nanostructures, *Mater. Chem. Phys.*, 275, 125211.

[82] Fang, Y., Liu, Q., and Zhu, S., 2021, Selective biosorption mechanism of methylene blue by a novel and reusable sugar beet pulp cellulose/sodium alginate/iron hydroxide composite hydrogel, *Int. J. Biol. Macromol.*, 188, 993–1002.

[83] Alagarsamy, A., Chandrasekaran, S., and Manikandan, A., 2022, Green synthesis and characterization studies of biogenic zirconium oxide (ZrO_2) nanoparticles for adsorptive removal of methylene blue dye, *J. Mol. Struct.*, 1247, 131275.